Cluster-Expansion Model for Complex Quinary Alloys: Application to Alnico Permanent Magnets

Manh Cuong Nguyen,[1,*] Lin Zhou,[1] Wei Tang,[1] Matthew J. Kramer,[1,2] Iver E. Anderson,[1,2] Cai-Zhuang Wang,[1,3] and Kai-Ming Ho[1,3]

[1]*Ames Laboratory, U.S. Department of Energy, Iowa State University, Ames, Iowa 50011, USA*
[2]*Department of Materials Science and Engineering, Iowa State University, Ames, Iowa 50011, USA*
[3]*Department of Physics and Astronomy, Iowa State University, Ames, Iowa 50011, USA*

(Received 27 February 2017; revised manuscript received 23 August 2017; published 8 November 2017)

An accurate and transferable cluster-expansion model for complex quinary alloys is developed. Lattice Monte Carlo simulation enabled by this cluster-expansion model is used to investigate temperature-dependent atomic structure of alnico alloys, which are considered as promising high-performance non-rare-earth permanent-magnet materials for high-temperature applications. The results of the Monte Carlo simulations are consistent with available experimental data and provide useful insights into phase decomposition, selection, and chemical ordering in alnico. The simulations also reveal a previously unrecognized $D0_3$ alloy phase. This phase is very rich in Ni and exhibits very weak magnetization. Manipulating the size and location of this phase provides a possible route to improve the magnetic properties of alnico, especially coercivity.

DOI: 10.1103/PhysRevApplied.8.054016

I. INTRODUCTION

An accurate and efficient configurational exploration scheme for complex multicomponent alloys has been considered as a difficult, long-standing problem in the design of complex alloys at finite temperature. Monte Carlo simulation [1] can be used to investigate the alloys at finite temperatures. However, an efficient and accurate method for energy calculation of large-size systems is a bottleneck. First-principles density-functional-theory (DFT) [2] calculations can give accurate energy, but the computational demand is too heavy to be feasible for practicing Monte Carlo simulation for complex alloys. Cluster expansion (CE) [3,4], which mimics the well-known spin Ising model with spin eigenvalues at each lattice site replaced by chemical occupations of the alloy constituents, offers a possible way to address this challenge for alloys having a defined underlying lattice. The model parameters called cluster-expansion coefficients are determined by fitting to the energies resulted from accurate calculations (e.g., DFT) of a set of training structures. Using the CE model, the energy of an alloy supercell containing thousands of lattice sites can be calculated within subseconds, making Monte Carlo simulation for complex multicomponent alloys feasible.

In principle, the CE model can be applied to alloys with any number of chemical elements as long as the underlying lattice is defined. In practice, the complexity of the method increases rapidly with the number of chemical elements in multicomponent alloys [4]. Most of the work with CE so far has been for binary and ternary systems [5–8] and far less has been for more components' alloy systems. There have been a few papers employing CE for quaternary and quinary alloys published so far [9–12].

Alnico alloys were the permanent-magnet (PM) materials of choice prior to the discovery of rare-earth (RE)-based alloys in the 1960s. Recently, alnico has received much attention because it is a promising candidate for further development of magnets for elevated- and high-temperature applications [13,14]. Alnico magnets have a very small temperature dependence for their magnetic properties [14], which is highly desirable for some applications such as traction motors used in electric vehicles where the working conditions include elevated temperatures of 420–480 K. Alnico 8 and 9 have coercivity $H_{ci} = 1900$ and 1375 Oe and remanence $B_r = 7.4$ and 11.2 kG, respectively, and can be further enhanced by modifying the microstructure or alloying [13–15] or via magnetothermal treatment processes. A redesign of the PM motor, specifically for using alnico together with an enhancement of alnico coercivity, can make non-rare-earth PM vehicle motors possible in the near future. Comprehensive knowledge about the structure changes at the atomic scale with the annealing temperature of alnico is essential for optimizing processing to control the microstructure of alnico and, thereby, to enhance its magnetic properties.

The general understanding of alnico is that the system consists of two primary alloy phases: the ferromagnetic (namely, α_1) phase rich in Fe and Co and the "nonmagnetic" matrix (namely, α_2) phase with Al, Ni, Co, and some Fe with minor alloying elements such as Ti. Both phases have a coherent body-centered-cubic (bcc) underlying lattice (the α_2 forms the $L2_1$ order, which can be considered as a supercell of eight bcc units). The segregation of the alnico

*mcnguyen@ameslab.gov

master alloy into the α_1 and α_2 phases arises from spinodal decomposition occurring during the cooling and quenching from a solid solution (bcc or $B2$) phase at very high temperature (approximately 1523 K). The best-performing alnico alloys require annealing with a magnetic field near their Curie temperature (approximately 1113 K for approximately 10 min) followed by a series of lower-temperature anneals (e.g., 883 or 863 K for a few hours) [16–18] where details vary based on composition. The subsequent morphology of the spinodal varies with composition. While alnico 5 and 5-7 show a "brick-and-mortar" pattern, alnico 8 and 9 show a "mosaic tile" pattern in the microstructures in a transverse section [15,19]. The purpose of the magnetic field annealing is to bias the growth of the spinodal phases along the applied field direction. The magnetic α_1 phase will form long needles separated by the matrix α_2 phase in those crystals whose [001] axis is well aligned to the magnetic field. It is the magnetic shape anisotropy of the α_1 phase that is responsible for the enhanced magnetism in these alloys. The α_2 phase is believed to be a nonmagnetic or weakly magnetic phase which decouples the interactions between the α_1 phase needles to enhance the shape anisotropy of the α_1 needles and, hence, the coercivity of alnico.

In this work, we develop a cluster-expansion model for bcc quinary alnico alloys consisting of Al, Ni, Co, Fe, and Ti based on a DFT structure database. The cluster-expansion model is intensively and extensively validated for temperature-dependent phase separation and chemical ordering of known ternary alloys. We use lattice Monte Carlo simulation to study the phase selection and chemical ordering in alnico 8 and 9. The decomposition into α_1 magnetic and α_2 matrix phases is more complete at lower annealing temperature. We show that there is an additional third alloy phase, which is rich in Ni. Our prediction of the third alloy phase is fully supported by experimental observation with high-resolution TEM. The chemical orderings and magnetic properties of all alloy phases are also investigated. The details of the computational methods and model are given in the Supplemental Material [20].

II. RESULTS AND DISCUSSIONS

We fit the CE coefficients for bcc quinary Al-Ni-Co-Fe-Ti alloy up to the third nearest-neighbor (NN) pair and triplet clusters by ATAT code [4,21] to a data set from DFT calculations [22–26]. Figure 1 shows the formation energies of the reference structures calculated by the CE model versus DFT. We can see that the CE energies are very well fitted to the DFT energies. The root-mean-square error of this fitting is very small, 12.9 meV/atom. The cross-validation score, which measures the error in predicting energies of a set of new structures that are not included in the reference database [4], is an important indicator of the accuracy and transferability of CE coefficients. As one can see from Fig. 1, the cross-validation score is also very small (17.2 meV/atom) in our CE model. We also show in Fig. 1

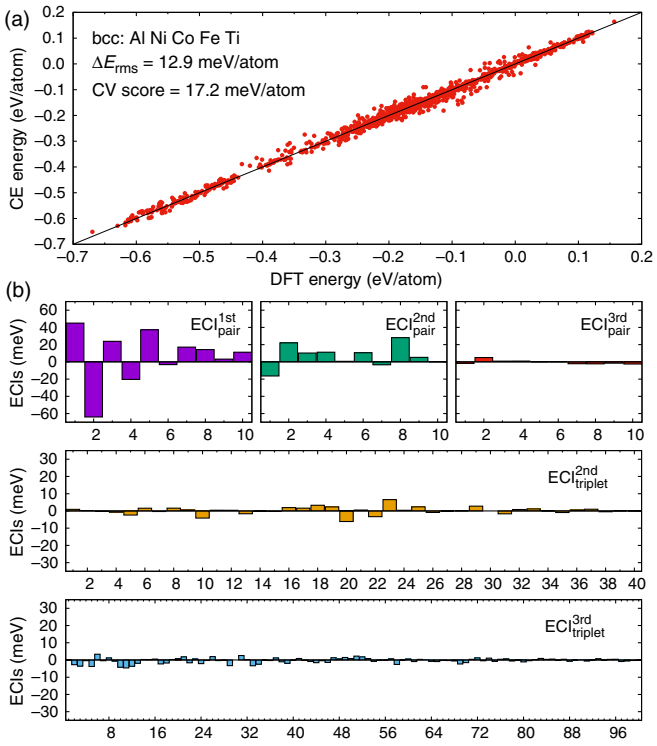

FIG. 1. CE vs DFT formation energies of database structures is shown in (a), and the values of the ECIs of first, second, and third NN pair and second and third NN triplet clusters are shown in (b). The horizontal x axis stands for different clusters having different chemical decorations.

the values of effective cluster interactions (ECIs) of the pair and triplet clusters obtained from our CE fitting. We can see that the first and second NN pair interactions are the most significant, whereas the ECIs of the third NN pair interactions and the triplet interactions are much smaller. This indicates that further increasing the number of clusters may not be needed.

We further validate our quinary CE model by describing the phase selection and decomposition in complex alloys by performing MC simulations for a wide range of temperatures for known bcc-based ternary alloys of Al, Ni, Co, Fe, and Ti: $AlNiFe_2$, $AlCo_2Ti$, and $AlNi_2Ti$ ternary alloys. $AlNiFe_2$ is in a $B2$ (AlFe, NiFe) single phase at high temperature and is decomposed into bcc Fe-rich and $B2$ NiAl-rich phases at low temperature [27]. $AlCo_2Ti$ and $AlNi_2Ti$ are in the $L2_1$ phase for a wide range of temperatures [28–30]. We show in Fig. 2 the calculated compositional contour histograms calculated from 1000 converged configurations of $AlNiFe_2$ ternary alloy at different temperatures, 773, 1173, and 1973 K, respectively. We can see clearly that the $AlNiFe_2$ alloy is in a single phase at high temperature (1973 K) and is decomposed into two phases, NiAl-rich and Fe-rich phases, at lower temperature (1173 and 773 K). From the neighbor correlation tables of the $AlNiFe_2$ alloy at high (1973 K) and low (773 K) temperature (Tables S.1 and S.2 in the Supplemental Material

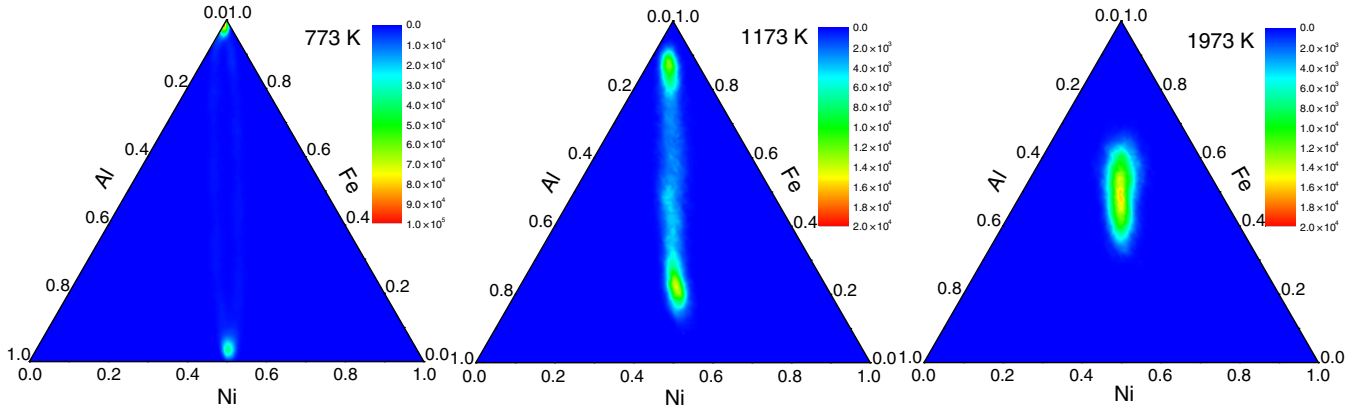

FIG. 2. Compositional contour histograms showing relative composition probabilities of $AlNiFe_2$ ternary alloy at different annealing temperatures obtained from MC simulation. Histograms are calculated from 1000 converged configurations.

[20]), we find that at high temperature, the $AlNiFe_2$ is in a $B2$ order with almost all Al atoms sitting on the α site and almost all Ni atoms sitting on the β site. At low temperature, the AlNi-rich phase is in $B2$ order with the α site occupied mostly by Al and the β site occupied mostly by Ni. These observations of temperature-dependent phase separation, phase selection, and phase ordering from our MC simulations are consistent with the experimental phase diagram [27]. However, there is an overestimation of the transition temperature from two phases to a single phase of $AlNiFe_2$ alloy. The transition temperature is about 1873 K in our MC simulation, while it is about 1273 K from the phase diagram. This overestimation of phase-transition temperature can be traced back to several factors including the truncation of CE coefficients, the systematic error in DFT calculations, and the contribution of vibrational entropy to free energy. We do not discuss this overestimation here in detail since previous works already discussed this overestimation of the transition temperature quite clearly [8,10]. Monte Carlo simulations for $AlCo_2Ti$ and $AlNi_2Ti$ ternary alloys (see the Supplemental Material [20]) show that both phases are in an $L2_1$ order phase for a wide range of temperatures, which is also consistent with experimental results [28–30]. Therefore, apart from an offset in transition temperature, the MC simulation based on the CE method can describe the phase selection and decomposition of complex alloys accurately. These results also validate the accuracy and transferability of our developed CE model for the quinary alloy.

The chemical composition of commercial alnico 8 (without Cu), i.e., $Al_{0.140}Ni_{0.117}Co_{0.359}$ $Fe_{0.312}Ti_{0.072}$, is used in our simulations for alnico. Figure 3 shows the compositions of the phases of alnico as a function of the annealing temperature between 773 and 1773 K. First, let us discuss the right part of the plot with temperature higher than 973 K. For temperature higher than 1573 K, the alnico master alloy is in a homogenized phase with the composition of each element as that of the overall composition. For temperature lower than 1573 K, the alnico master alloy decomposes into two phases. It is interesting that the decompositions of constituent elements start at different temperatures: Al, Fe, and Ti start to split their compositions first between 1473 and 1573 K then Co and Ni start to split their compositions between 1273 and 1373 K. The late decomposition of Co was also observed in MC simulations for alnico 5-7 [10].

The two decomposed phases are the magnetic α_1 and matrix α_2 phases, respectively. From Fig. 3, we can see that the compositions of Al, Ni, and Ti in the α_1 phase and those of Fe and Co in the α_2 phase are decreasing as the annealing temperature decreases. At lower temperature (1073 or 973 K), the compositions of Al and Ni in the α_1 phase are very small, and there is almost no Ti in the α_1 phase. In the α_2 phase, the compositions of Co are less but still considerable, and the Fe drops off more but goes to about half the starting level. These results are consistent with the experimental results for alnico 8 and 9: Ti is mostly residing in the α_2 phase with very small or almost no Ti in

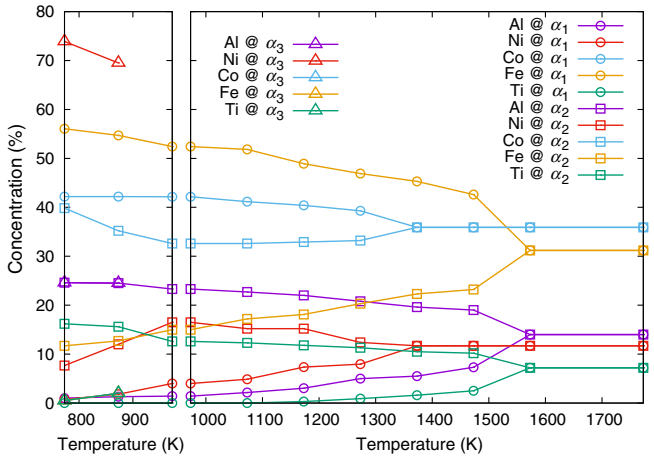

FIG. 3. Composition of each element in alnico 8 as a function of annealing temperature obtained from MC simulations. Circle, square, and up triangle symbols are for compositions of the α_1, α_2, and α_3 phases.

the α_1 phase; the α_1 phase consists mainly of Fe and Co with small amounts of Ni and Al; the concentration of Fe and Co in the α_2 phase is still significant, with Co only slightly less than in the α_1 phase. Because Ni is a very weak magnetic element, the magnetism of the magnetic α_1 phase is enhanced if the concentration of Ni is low. On the other hand, the coercivity of alnico 8 and 9 is enhanced if the α_2 matrix phase is less magnetic or nonmagnetic to properly decouple the interactions between the magnetic α_1 phase needles. The results shown in Fig. 3 imply that lowering the annealing temperature can improve the magnetic properties of alnico by enhancing the magnetism of the α_1 phase via increasing the magnetic elements' concentrations while diminishing the magnetism of the α_2 phase via decreasing the magnetic elements' concentrations at the same time.

The compositions of the α_1 and α_2 phases obtained from MC simulations between 973 and 1173 K are quite close to the experimental observations for alnico 8 [15], especially the α_1 phase. There is an overestimation of the Fe composition and an underestimation of the Ni composition in the α_2 phase. The differences can be attributed to two main factors. First, our MC simulation is for the equilibrium state, meaning that the observed compositions from simulation are at the boundaries of the spinodal decomposition domain. Heat treatment in an experiment is only for a short time so that the measured compositions of decomposed phases diverge to points along the horizontal line connecting the two end (equilibrium) points of the spinodal decomposition domain at the given temperature and not the end points. Second, although DFT is currently one of the state-of-the-art first-principles methods, it can have a systematic error in the relative stabilities of different alloy phases. For a quinary alloy, there are too many possible suballoy phases so that it is not feasible to trace back for the DFT systematic error, and a small underestimation or overestimation of the compositions of constituent elements in the α_1 and α_2 phases is understandable and actually expected in our simulations. We also like to note that we observe a temperature offset, in comparison with experiment, in the MC simulation for the ternary discussed above. A temperature offset should be also expected for alnico alloys. Since the current work focuses on the trend of the phase decomposition and ordering in alnico 8 and 9 as a function of the annealing temperature rather than the exact compositions of each separated phase at a given temperature, the results obtained from our MC simulations provide very valuable information on the relative order of reactions for designing optimal heat treatment processes in experiment.

Commercial alnico 8 and 9 magnets achieve their current reproducible properties through the above-mentioned complex processes that include quenching and annealing (with and without external field) at different temperatures for different periods of time [18]. This complicated process scheme came from experimental experiences accumulating over a long period of time, essentially for 70–80 years. However, the urgent need for improvement of the magnetic properties of alnico alloys for use in compact electric drive motors needs a better approach than the time-consuming blind trial-and-error experimentation efforts. A better understanding of the physics behind the current multistep annealing processing should be the first move forward to speed up the cycle for improved magnetic properties of alnico. The results in Fig. 3 give us some key information for better understanding of the dependence of structures and magnetic properties of the synthesis processes. As shown in Fig. 3, the spinodal decomposition can involve very significant compositional shifts, but the extent of this transformation that takes place during fast quenching and high-temperature annealing depends on atomic mobility to establish the overall microstructure of the *mosaic tile* pattern. The spinodal decomposition evolves faster at higher temperature so that the first magnetic annealing step needs to be at a high temperature (just below the spinodal onset and the Curie temperature of the α_1 phase) to rapidly generate the mosaic microstructure. Unfortunately, the Co (Ni) composition is the same or very close in the α_1 and α_2 phases at high temperature, meaning that the Co (Ni) concentration is too high in the α_2 (α_1) phases. A high Co concentration in the α_2 phase can induce magnetism in the α_2 phase and, hence, lower the coercivity due to poor magnetic isolation between the α_1 phase needles. At the same time, high Ni concentration in the α_1 phase will lower the magnetic moment of the α_1 phase. As a result, the magnetization and coercivity of alnico 8 and 9 right after high-temperature magnetic annealing are low. The lower-temperature annealing (draw process) has the effect of altering the Ni and Co compositions in the α_1 and α_2 phases. It is desirable that these annealing steps significantly lower the unwanted high Co concentration in the α_2 phase and the overall Ni content in the α_1 phase to enhance the magnetic properties of alnico 8 and 9. However, the spinodal decomposition evolves much slower at lower temperature so that a very long time of annealing is needed to obtain the desired microstructure for good magnetic properties.

We also find that if the annealing temperature is further lowered to below 973 K (left part of Fig. 3), there is a third alloy phase appearing in the alnico system. We refer to this apparently distinct phase as the α_3 phase. This α_3 phase consists of mainly Ni and Al with very low concentrations of other transition-metal elements [e.g., $Ni_{0.73}Al_{0.25}(FeCoTi)_{0.02}$ at 773 K]. In Fig. 4, we show the composition profiles of each element along the z direction of the simulation supercell obtained from MC simulations at 973 and 823 K. The compositions of each element at a given z value is calculated as the average of the composition of that element on all sites at that z value. It is interesting that the concentration of Al is almost constant crossing the α_2 and α_3 phases, indicating that the concentration of Al may be possible to manipulate the volume

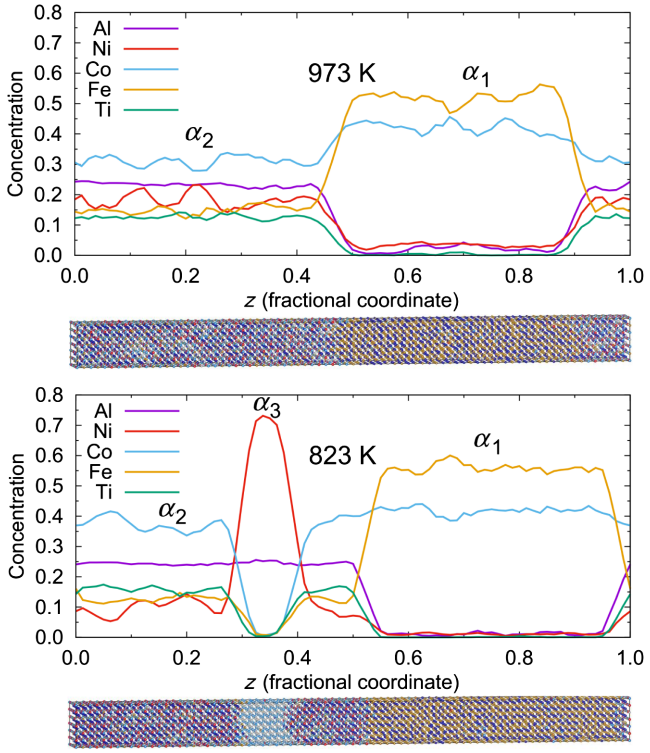

FIG. 4. Composition profile of alnico 8 along the z direction and the corresponding real-space atomic structure obtained from MC simulations at (top) 973 K and (bottom) 823 K. The silver, light green, blue, gold, and red balls in the crystal structure (band beneath each composition profile) indicate the Al, Ni, Co, Fe, and Ti atoms.

fraction of the α_1 magnetic phase in alnico. There could be several reasons why α_3 phase was not recognized. First, the α_3 phase appears only at quite low annealing temperature in our MC simulations, meaning that it may need a very long annealing at a low temperature in an experiment to grow to a large enough size to be detectable. The typical time for each step of the low-temperature draw process is from several hours to half a day [18], which may not be long enough. Second, there can be a high kinetic barrier blocking the formation of the α_3 phase, although it is thermodynamically stable. Annealing at low temperature does not provide enough kinetics to overcome the barrier. Therefore, the α_3 phase can be quite small in size in comparison to the α_1 and α_2 phases so that it cannot be seen clearly in the characterization experiment that focuses on the micron-scale structure of alnico 8 and 9 [15,19]. The identification of the α_3 phase in alnico is possible only when all five chemical elements are taken into account, showing that quinary CE is indeed needed to study alnico 8 and 9.

We perform kinetically limited Monte Carlo simulations to understand the effects of short annealing time and slow kinetics at low annealing temperature on the morphology of the structures. Starting with the equilibrium configuration of a high-temperature MC simulation (1473 K) as the initial configuration (Fig. S.2 [20]), we swap only two randomly picked atoms separated by a distance smaller than 5 or 10 times the lattice constant of a bcc unit cell. These limited swapping ranges are used to mimic the slow diffusion of atoms in alnico during low-temperature annealing. With such simulations, we indeed observe the α_3 phase, which has an Al-to–transition-metal (Fe, Co, and Ti together) composition ratio of 1:3, and Ni is richer than all other transition metals. The concentration of Ni increases with the number of MC steps until reaching the saturated concentration. The concentration for Ni in the α_3 phase varies from approximately 30% to approximately 75%, depending on the simulation, and the α_3 phase is usually quite small along the z direction of a simulation supercell. If we release the constraint on swapping distance, we can obtain the results that we discuss above, where there is almost no Fe, Co, and Ti in the α_3 phase. These results show that the Ni-rich α_3 phase in real alnico samples has a general TM-to-Al ratio of 3:1 and is small in size, which is consistent with the observation of a Ni-enriched rod-shaped phase in commercial alnico 9 [31]. Cu-rich and Ni-rich bridges were also observed in lab alnico samples with composition close to those of commercial alnico 8 and 9 [32], and our results should also be noted for commercial alnico 8 showing Ni-rich clusters or phases (see the Supplemental Material [20]). More studies may be needed to clarify the relationship between observed Ni-enriched clusters or phases with the α_3 phase. The success of predicting an alloy phase in a complicated multicomponent alloy at finite temperature in this work is a significant achievement for theoretical materials prediction and design. Most of the theoretical predicted and designed materials so far are binary or ternary alloys stabilized at zero temperature.

Now let us consider the chemical ordering of five constituent elements in the α_1, α_2, and α_3 phases of alnico 8 and 9 based on the Bragg-William definition of the degree of order [33]. We consider the ordering of the α_1 phase first. From the obtained correlation table (Table S.5 [20]), we observe that the local environment of Fe and Al (Co and Ni) are very similar, as both of them have very similar numbers of first NN and second NN to other elements, suggesting that if the α_1 phase is in $B2$ or $D0_3$ order, Fe and Al (Co and Ni) will be in the same sublattice. Most of the Ti first NNs are Ni and Co (7.50 out of 8.00) so that Ti should be on the same sublattice with Fe and Al. Therefore, we consider Fe, Al, and Ti (Co and Ni) identical in estimating the ordering of the α_1 phase. From our occupation scanning, the α_1 phase has $B2$ order with a degree of order of 77.9% at 773 K, and it decreases with the temperature, e.g., 52.8% at 973 K and 43.8% at 1173 K.

From the correlation table of the α_2 phase at 973 K (Table S.6 [20]), we can find that there is no Al-Al and Al-Ti first NN or almost no Al-Al second NN, meaning that the α_2 phase is not in the disordered bcc structure. If the α_2

phase is in $B2$ order, all Al and Ti should be in the same sublattice because there is no Al-Al and Al-Ti first NN. Then, Al and Ti should be the second NN to themselves and to each other. But there is almost no Al-Al and Ti-Ti second NN, indicating that the α_2 phase is not in the $B2$ order. The fact that there is no Al-Al and Al-Ti first NN, that there is almost no Al-Al and Ti-Ti second NN, that almost all second NNs of Al are Fe and Ti (5.64 out of 6.00), and that almost all third NNs of Al are Al (10.93 out of 12.00) suggest that the α_2 should be in an $L2_1$ order with all Al on the $4a$ site and Fe and Ti on the $4b$ site. There can be some antisite defects, and the composition of the α_2 phase is not $L2_1$ stoichiometry [i.e., (NiCo):(FeTi):Al is not a 2:1:1 ratio] so that there are some small Al-Ni and Al-Co second NNs, or the number of Al-Al third NNs is not exactly 12.0. Therefore, we can group the five elements into three groups Ni + Co, Fe + Ti, and Al to calculate the correlation table of the "pseudoternary." Because there are absolutely no Al-Al first NNs and a very small number of Al-Al second NNs, we can assume (in order to make the estimation of degree of order easier) that all Al of the pseudoternary is on the $4a$ site of $L2_1$ order if the concentration of Al is less than or equal to 0.25. We then vary the occupations of the other two groups on the rest of the three sites, i.e., $4a$, $4b$, and $8c$ sites, to find the best matching correlation table to the target table calculated for the pseudoternary. The degree of order is then estimated as the degree of order of (Ni + Co) and (Fe + Ti) on the $8c$ and $4b$ sites. Our calculation shows that the degree of order of the $L2_1$ α_2 phase is very high, and it is decreasing with the temperature, e.g., 99.2% at 773 K, 92.8% at 973 K, and 84.8% at 1173 K. The decrease of the degrees of order of the α_1 and α_2 phases is coming directly from the increasing of antisite defects with the temperature. Our simulation results related to ordering of the α_1 and α_2 phases are in agreement with recent experiments using advanced atomic scale energy-dispersive x-ray-spectra mapping techniques [34].

Let us now consider the ordering of the identified α_3 phase. The correlation table at 773 K shows clearly that the α_3 phase is not in the disordered bcc phase as there is absolutely no Al-Al first NN. Thus, the α_3 phase should be in a $B2$ or $D0_3$ order. The number of first NNs of Fe and Ti to Al is almost zero so that we can place Co in the same group with Ni and Fe, and that Ti is in the same group with Al for the α_1 phase case. The correlation table of pseudobinary Ni-Al is shown in Table S.7 of Ref. [20]. Our occupation scanning shows that the α_3 phase is in a $D0_3$ order with a very high degree of order for both temperatures where we observe the α_3 phase, i.e., 99.5% at 773 K and 99.0% at 873 K.

The magnetic moment per lattice site from the DFT calculation within coherent-potential approximation [35–37] as a function of the annealing temperature for the α_1 and α_2 phases is shown in Fig. 5(a). We can see that the magnetic moment of the α_1 phase is decreasing with the annealing temperature. In contrast, the magnetic moment of the α_2 phase is increasing with the annealing temperature. This variation of the magnetic moment of the α_1 (α_2) phase comes directly from the decrease (increase) of the magnetic element (Fe and Co) concentrations in the α_1 (α_2) phase with the annealing temperature. In both phases, the magnetic moments of Fe, Co, and Ni are ferromagnetically coupled, while coupling between Ti and other magnetic elements is antiferromagnetic. The magnetic moments of Fe and Co are dominant, and they are almost constant in each phase, e.g., approximately 2.75 (approximately 2.50) μ_B/atom and approximately 1.82 (approximately 1.74) μ_B/atom for Fe and Co on the $\alpha(\beta)$ site in the α_1 phase and approximately 2.85 μ_B/atom for Fe on the $4b$ site and approximately 0.84 for Co on the $8c$ site in the α_2 phase. The magnetic moment of Ti is approximately -0.50 μ_B/atom in the α_2 phase. The magnetic moment of Ni is approximately 0.62 μ_B/atom in the α_1 phase and approximately 0.20 μ_B/atom in the α_2 phase. These results are similar to those of alnico 5-7 [9]. However, the concentration of Co in alnico 5-7 is much smaller than that in alnico 8, making a much smaller magnetic moment for the α_2 phase in alnico 5-7, about half of that in alnico 8, which is considered here. Figure 5(b) shows the magnetic moment of the α_3 phase with Ni substituted for other TMs: $D0_3$ $(Ni_{1-3x}Fe_xCo_xTi_x)_3Al$ with $0 \leq \times \leq 0.2$. For simplicity, we assume the same concentrations for Fe, Co, and Ti. The magnetic moment of the α_3 phase increases monotonically with the concentration of other TMs on the Ni sites. For $x > 0$, Fe, Co, and Ni also exhibit ferromagnetic coupling among themselves and antiferromagnetically coupled with Ti. The magnetic moment of Fe and Co is dominant, i.e., at $x = 0.20$ the magnetic moments of Fe, Co, Ni, and Ti are 1.92, 0.87, 0.12, and -0.21 μ_B/atom, respectively. At very high substitution concentration ($x = 0.20$), the magnetic moment of the α_3 phases is still small (0.41 μ_B/site), which is much smaller than that of the α_1 phase and about two-thirds that of the α_2 phase at 773 K.

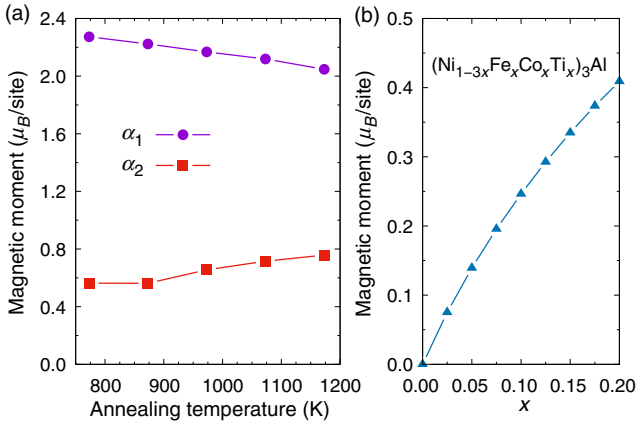

FIG. 5. Magnetic moments of the (a) α_1 and α_2 phases as a function of annealing the temperature and (b) that of the α_3 phase as a function of TM content in the Ni site.

The above MC simulations and magnetic calculations show that magnetism in the α_2 phase is inevitable due to high Co concentration in the α_2 phase. The magnetism of the α_2 phase lessens the magnetic isolation between needles of the α_1 phase and lowers the coercivity of alnico, as we mention above. The identified α_3 phase appearing at low annealing temperature provides a clue for a possible way to overcome the magnetism issue in the α_2 phase. If we can achieve the enrichment of Ni in the α_3 phase precipitating at the boundary of the α_1 and α_2 phases during low-temperature annealing, a very weak magnetic "skin layer" will be developed to wrap the α_1 needles. Hence, the α_1 magnetic needles will be magnetically well decoupled from each other, then the coercivity of alnico will be enhanced. Recent experimental work on alnico showed the signal of this skin layer [32]. Our results suggest that the substitution of Co by Ni or cosubstitution of Co by Ni-Fe or Ni-Al pairs, a similar concept of codoing in semiconductors, to lower the Co concentration and provide more Ni for the α_3 phase to develop, together with a redesign of the draw process to include lower-temperature annealing will enhance the formation of the α_3 phase. This substitution can reduce unwanted Co in the α_2 phase and also lower the cost of alnico, as Co is more costly than other metals like Fe, Al, and Ni in alnico.

III. SUMMARY

In summary, we develop an accurate and transferable quinary alloy cluster-expansion model. Monte Carlo simulations are performed to study the atomic structures of alnico 8 and 9 at atomistic and nanoscales as a function of the annealing temperature. The simulation results of phase separation and phase selection are in agreement with experiment. More details on the ordering in each separated phase of alnico are provided: the α_1 phase is in $B2$ order with Ni and Co preferring the same sublattice site; the α_2 phase is in $L2_1$ order with Ni and Co preferring the $8c$ site and Al occupying the $4a$ site. A third alloy phase is predicted by Monte Carlo simulations and confirmed by experiment. The alloy phase is rich in Ni, has a TM:Al ratio of 3:1 in general, is in $D0_3$ TM_3Al order, and exhibits very weak magnetization. The identification of the α_3 phase gives a possible route to enhance magnetic properties of alnico by controlling the processing conditions to manipulate the size and locations of the α_3 phase.

ACKNOWLEDGMENTS

The U.S. Department of Energy, Office of Energy Efficiency and Renewable Energy, Vehicle Technologies Office, Electric Drive Technologies Program supports the research at the Ames Laboratory, which is operated for the DOE by Iowa State University under Contract No. DE-AC02-07CH11358. We also acknowledge computing time support at the National Energy Research Scientific Computing Center.

[1] N. Metropolis and S. Ulam, The Monte Carlo method, J. Am. Stat. Assoc. **44**, 335 (1949).
[2] W. Kohn and L. J. Sham, Self-consistent equations including exchange and correlation effects, Phys. Rev. **140**, A1133 (1965).
[3] J. M. Sanchez, F. Ducastelle, and D. Gratias, Generalized cluster description of multicomponent systems, Physica A (Amsterdam) **128A**, 334 (1984).
[4] A. van de Walle, Multicomponent multisublattice alloys, nonconfigurational entropy and other additions to the Alloy Theoretic Automated Toolkit, CALPHAD Comput. Coupling Phase Diagrams Thermochem. **33**, 266 (2009).
[5] C. Wolverton and D. de Fontaine, Cluster expansions of alloy energetics in ternary intermetallics, Phys. Rev. B **49**, 8627 (1994).
[6] A. Van der Ven and G. Ceder, Vacancies in ordered and disordered binary alloys treated with the cluster expansion, Phys. Rev. B **71**, 054102 (2005).
[7] J. S. Wróbel, D. Nguyen-Manh, M. Y. Lavrentiev, M. Muzyk, and S. L. Dudarev, Phase stability of ternary fcc and bcc Fe-Cr-Ni alloys, Phys. Rev. B **91**, 024108 (2015).
[8] F. Lechermann, M. Fahnle, and J. M. Sanchez, First-principles investigation of the Ni-Fe-Al system, Intermetallics **13**, 1096 (2005).
[9] W. P. Huhn and M. Widom, Prediction of A2 to B2 phase transition in the high-entropy alloy Mo-Nb-Ta-W, JOM **65**, 1772 (2013).
[10] M. C. Nguyen, X. Zhao, C.-Z. Wang, and K.-M. Ho, Cluster expansion modeling and Monte Carlo simulation of alnico 5-7 permanent magnets, J. Appl. Phys. **117**, 093905 (2015).
[11] S. B. Maisel, M. Höfler, and S. Müller, Configurationally exhaustive first-principles study of a quaternary superalloy with a vast configuration space, Phys. Rev. B **94**, 014116 (2016).
[12] I. Toda-Caraballo, J. S. Wróbel, S. L. Dudarev, D. Nguyen-Manh, and P. E. J. Rivera-Díaz-del-Castillo, Interatomic spacing distribution in multicomponent alloys, Acta Mater. **97**, 156 (2015).
[13] R. W. McCallum, L. Lewis, R. Skomski, M. J. Kramer, and I. E. Anderson, Practical aspects of modern and future permanent magnets, Annu. Rev. Mater. Res. **44**, 451 (2014).
[14] M. J. Kramer, R. W. McCallum, I. A. Anderson, and S. Constantinides, Prospects for non-rare earth permanent magnets for traction motors and generators, JOM **64**, 752 (2012).
[15] L. Zhou, M. K. Miller, P. Lu, L. Ke, R. Skomski, H. Dillon, Q. Xing, A. Palasyuk, M. R. McCartney, D. J. Smith, S. Constantinides, R. W. McCallum, I. E. Anderson, V. Antropov, and M. J. Kramer, Architecture and magnetism of alnico, Acta Mater. **74**, 224 (2014).
[16] J. W. Cahn, On spinodal decomposition, Acta Metall. **9**, 795 (1961).
[17] J. W. Cahn, Magnetic aging of spinodal alloys, J. Appl. Phys. **34**, 3581 (1963).
[18] M. Stanek, L. Wierzbicki, and M. Leonowicz, Investigations of thermo-magnetic treatment of alnico 8 alloy, Arch. Metall. Mater. **55**, 571 (2010).
[19] Q. Xing, M. K. Miller, L. Zhou, H. M. Dillon, R. W. McCallum, I. E. Anderson, S. Constantinides, and M. J. Kramer, Phase

and elemental distributions in alnico magnetic materials, IEEE Trans. Magn. **49**, 3314 (2013).

[20] See the Supplemental Material at http://link.aps.org/supplemental/10.1103/PhysRevApplied.8.054016 for details of computational methods and model, extra validation of quinary cluster expansion model, neighbor correlation tables of ternary and alnico, results of kinetically-limited Monte Carlo simulation and experimental result.

[21] A. van de Walle and G. Ceder, Automating first-principles phase diagram calculations, J. Phase Equilib. **23**, 348 (2002).

[22] G. Kresse and J. Furthmüller, Efficient iterative schemes for ab initio total-energy calculations using a plane-wave basis set, Phys. Rev. B **54**, 11169 (1996).

[23] P. E. Blöchl, Projector augmented-wave method, Phys. Rev. B **50**, 17953 (1994).

[24] G. Kresse and D. Joubert, From ultrasoft pseudopotentials to the projector augmented wave method, Phys. Rev. B **59**, 1758 (1999).

[25] J. P. Perdew, K. Burke, and M. Ernzerhof, Generalized Gradient Approximation Made Simple, Phys. Rev. Lett. **77**, 3865 (1996).

[26] H. J. Monkhorst and J. D. Pack, Special points for Brillouin-zone integrations, Phys. Rev. B **13**, 5188 (1976).

[27] P. B. Budberg and A. Prince, in edited by G. Petzow and G. Effenberg, *Ternary Alloys* (VCH, Weinheim, 1991), pp. 309–323.

[28] V. Y. Markiv, Phase equilibrium in the Ti-Co-Al system, Russ. Met. **1**, 84 (1966).

[29] J. J. Ding, P. Rogl, and H. Schmidt, Phase relations in the Al-rich corner of the Ti-Ni-Al system, J. Alloys Compd. **317–318**, 379 (2001).

[30] K. Zeng, R. Schmid-Fetzer, B. Huneau, P. Rogl, and J. Bauer, The ternary system Al-Ni-Ti part II: Thermodynamic assessment and experimental investigation of polythermal phase equilibria, Intermetallics **7**, 1347 (1999).

[31] L. Zhou, M. Miller, D. A. Cullen, P. Lu, R. W. McCallum, I. E. Anderson, S. Constantinides, and M. J. Kramer, Microstructural characterization of alnico 9 alloy, Microsc. Microanal. Microstruct. **21**, 1343 (2015).

[32] M. Fan, Y. Liu, R. Jha, G. S. Dulikravich, J. Schwartz, and C. Koch, On the formation and evolution of Cu-Ni-rich bridges of alnico alloys with thermomagnetic treatment, IEEE Trans. Magn. **52**, 1 (2016).

[33] W. L. Bragg and E. J. Williams, The effect of thermal agitation on atomic arrangement in alloys, Proc. R. Soc. A **145**, 699 (1934).

[34] P. Lu, L. Zhou, M. J. Kramer, and D. J. Smith, Atomic-scale chemical imaging and quantification of metallic alloy structures by energy-dispersive x-ray spectroscopy, Sci. Rep. **4**, 3945 (2014).

[35] R. J. Elliott, J. A. Krumhansl, and P. L. Leath, The theory and properties of randomly disordered crystals and related physical systems, Rev. Mod. Phys. **46**, 465 (1974).

[36] H. Ebert *et al.*, Munich SPRKKR package, version 6.3, 2012.

[37] H. Ebert, D. Ködderitzsch, and J. Minár, Calculating condensed matter properties using the KKR-Green's function method—Recent developments and applications, Rep. Prog. Phys. **74**, 096501 (2011).